Molecular Adsorption Changes the Quantum Structure of Oxide-Supported Gold Nanoparticles: Chemisorption versus Physisorption

Christian Stiehler,[1] Florencia Calaza,[1] Wolf-Dieter Schneider,[1,2] Niklas Nilius,[1,3,*] and Hans-Joachim Freund[1]
[1]*Fritz-Haber-Institut der MPG, Faradayweg 4-6, 14195 Berlin, Germany*
[2]*Ecole Polytechnique Fédérale de Lausanne, CH-1015 Lausanne, Switzerland*
[3]*Carl von Ossietzky Universität, 26111 Oldenburg, Germany*

(Received 25 February 2015; revised manuscript received 11 May 2015; published 14 July 2015)

STM conductance spectroscopy and mapping has been used to analyze the impact of molecular adsorption on the quantized electronic structure of individual metal nanoparticles. For this purpose, isophorone and CO_2, as prototype molecules for physisorptive and chemisorptive binding, were dosed onto monolayer Au islands grown on MgO thin films. The molecules attach exclusively to the metal-oxide boundary, while the interior of the islands remains pristine. The Au quantum well states are perturbed due to the adsorption process and increase their mutual energy spacing in the CO_2 case but move together in isophorone-covered islands. The shifts disclose the nature of the molecule-Au interaction, which relies on electron exchange for the CO_2 ligands but on dispersive forces for the organic species. Our experiments reveal how molecular adsorption affects individual quantum systems, a topic of utmost relevance for heterogeneous catalysis.

DOI: 10.1103/PhysRevLett.115.036804 PACS numbers: 73.22.Dj, 68.37.Ef, 68.47.Jn, 73.20.Hb

Oxide-supported metal nanoparticles are pivotal elements in many heterogeneous catalysts used in industrial and environmental applications. Their reactivity maximum often lies in the so-called nonscalable size regime, in which the physical and chemical properties of the deposits strongly deviate from the known bulk behavior [1,2]. A key example concerns the high catalytic activity of nanosized gold over TiO_2 in the low-temperature CO oxidation [3]. The effect has been ascribed to a breakdown of the metallic band structure and the opening of gaps in the local density of states (LDOS) of the Au deposits [4].

Elucidating the origin of the unique catalytic response of supported nanoparticles is often hampered by the complexity of the respective materials. Even on uniform model systems [5,6], metal particles exhibit a broad size and shape distribution, being governed by structural irregularities of the oxide support. As a result, electronic characterization of unique deposits is impossible by spatially averaging spectroscopic techniques, and local approaches, such as electron [7,8] or scanning-tunneling microscopy (STM) need to be employed. Especially, the latter has demonstrated its enormous potential to unravel quantization patterns in spatially confined electronic systems [9,10], and the opening of LDOS gaps in particles of decreasing size [11,12].

However, also single-cluster techniques are often unable to catch the full complexity of electronic processes associated with chemical reactions. The reason is the flexibility of small electron systems under the impact of molecular adsorption [13]. Thereby, not only the metal deposits govern the binding state of the molecular ligands, for instance, via an electron-induced activation [14], but vice versa the particles electronic system is perturbed by the adsorbates. In fact, many chemical processes rely on a mutual electron exchange between educts and the catalyst surface. *In situ* monitoring of an adsorbate-induced reorganization of a finite electronic system is, however, challenging, as most spatially resolving techniques are sensitive to the high gas loads and temperatures during a chemical reaction. The present knowledge on such processes therefore relies on ensemble measurements, as performed with high-pressure XPS [15].

In the present work, we have circumvented such limitations by exploring the LDOS of one and the same metal nanoparticle with and without molecules attached to its surface. Our model system comprises monolayer Au islands grown on MgO thin films, which exhibit pronounced quantization effects accessible to low-temperature STM [11,12]. The confined electronic system is perturbed by dosing two molecular species onto the sample, CO_2 as a typical Lewis acid, and isophorone ($C_9H_{14}O$) as a weakly interacting hydrocarbon. The two molecules have an opposite impact on the quantum well states (QWSs) of the Au deposits, reflecting differences in the underlying binding mechanism.

All experiments were carried out with an ultrahigh-vacuum STM operated at 5 K. The sample electronic structure was probed with differential conductance (dI/dV) spectroscopy using a lock-in technique ($V_{\mathrm{mod}} =$ 15 mV rms). The MgO films were prepared by reactive Mg deposition onto a sputtered and annealed Ag(001) surface in 5×10^{-7} mbar O_2 at 550 K. The procedure resulted in atomically flat oxide layers, exposing large rectangular terraces delimited by nonpolar step edges [16,17]. About 0.06 ML of gold was evaporated onto the MgO surface at 300 K, where it aggregated into quasihexagonal islands

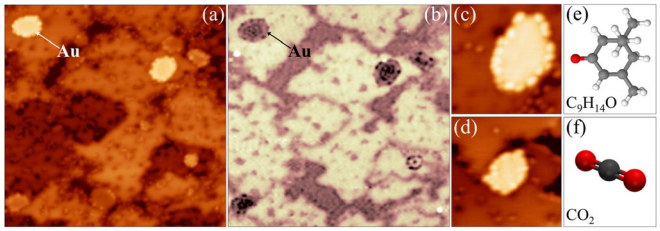

FIG. 1 (color online). (a) STM topographic image and (b) conductance map of Au islands on the MgO/Ag(001) thin film after isophorone exposure (60×60 nm^2, 1.7 V, 50 pA). The quantization pattern of the monolayer islands is clearly discernable in (b). Topographic images of (c) isophorone and (d) CO_2 molecules bound to Au clusters and the MgO surface (15×15 nm^2). Respective structure models are depicted in (e) and (f) (red color refers to oxygen).

of monolayer height. This peculiar 2D growth regime was ascribed earlier to an electron transfer from the low-work-function MgO/Ag support through the MgO spacer into the highly electronegative Au islands [Fig. 1(a)] [18]. The extra charges localize at the island perimeter, as this configuration minimizes repulsive electron-electron interactions [19]. Isophorone (0.5 L) was dosed at room temperature from a flask containing the liquid compound, while CO_2 (50 L) was supplied by backfilling the chamber with 1×10^{-7} mbar at 250 K sample temperature. After preparation, the sample was immediately transferred into the cryonic microscope to avoid contamination from the rest gas.

Figure 1 shows STM topographic and dI/dV images of the Au/MgO system after isophorone exposure. The scan was taken at +1.7 V, a bias at which the oxide film features a distinct metal-oxide interface state [17]. Given the high conductance associated with this state, MgO mono- and bilayers appear bright and become distinguishable from uncovered Ag and thick oxide patches in the dI/dV maps [Fig. 1(b)]. Hexagonal Au clusters of 15–35 nm^2 size are found on top of the oxide terraces. They are readily identified by their brightness in the topographic channel and by a pronounced quantization pattern in the conductance maps [12]. After isophorone dosage, circular protrusions of 1 nm diameter appeared on both the bare MgO and the Au islands. The new maxima have been assigned to the organic molecules with the help of their characteristic HOMO-LUMO signature. Remarkably, the Au-bound molecules were found exclusively along the island perimeter and no features have been detected in the interior. Along the island edges, the molecules have a regular spacing of about 1 nm, a value that coincides with the apparent size of isophorone. Each nanostructure therefore provides room for 10–20 edge-bound molecules [Fig. 1(c)]. A similar picture is observed after CO_2 dosing onto the Au/MgO surface [Fig. 1(d)]. Also, here the CO_2 molecules bind exclusively to the island perimeter and no ad-species are found within the nanostructures. The CO_2 species are also evenly spaced along the Au/MgO edge, however, with reduced periodicity in agreement with the smaller molecular diameter.

In a next step, we have explored the impact of molecular adsorption on the particles electronic structure. As shown before [11,12], planar Au islands containing 15–200 atoms develop pronounced QWSs, arising from hybridization of the Au $6sp$ atomic orbitals. Their energy position is determined either from deconvoluting STM conductance spectra into Gaussians or from fitting energy-resolved dI/dV maps to idealized eigenfunctions of a particle-in-a-box model [20]. Details of the procedure can be found in the Supplemental Material [21]. The influence of molecular adsorption is now deduced by comparing data sets taken on islands with molecules and after desorbing them with a voltage pulse [25]. Whereas isophorone could be reproducibly removed at 4.5 V sample bias without altering the island perimeter, CO_2 desorption turned out to be unreliable even at higher bias and sometimes led to drastic changes in the appearance of the islands. We have therefore referenced CO_2-related conductance data to spectra obtained on Au islands of similar size and shape before molecular dosage. This approach was approved in an earlier study, which analyzed the correlation between geometry and electronic structure of 2D quantum systems [26].

Figure 2 displays an Au island of about 220 atoms, before and after desorbing the 15 isophorone molecules from its perimeter. Successful removal of the ad-species is evident from subsequent STM images, although a few undefined residuals remained on the surface. The molecular desorption was accompanied by distinct changes in the electronic structure. The initial dI/dV curves, taken at different positions within the island, have been deconvoluted into five Gaussians localized at 0.7, 0.8, 1.1, 1.4, and 1.6 V, hence inside the energy window of the Au $6p_z$ manifold [19]. The symmetry of the quantization patterns was revealed from dI/dV mapping, showing a series of bright and dark ellipses that emerged from the island center and propagated outward with increasing bias [Figs. 2(a) and 2(d)]. While the lowest QWS at 0.7 V shows uniformly high dI/dV intensity, higher states are characterized by up to three dark and bright rings parallel to the island perimeter. The intensity patterns match the eigenstates of a hexagonal potential well, as described in Ref. [27]. Moreover, their bias evolution is in line with the QWS energies derived from the spectroscopic mode (see details in the Supplemental Material [21]). Note that the isophorone molecules themselves feature interesting intensity modulations, reflecting local differences in their binding characteristic at the metal-oxide boundary.

While the overall electronic structure of the Au island, e.g., the number and symmetry of the QWSs, remains unchanged after desorbing the molecular species, the energy of the eigenstates shifts in a characteristic manner. The trend is best discernable in the conductance maps of Fig. 2. For example, the 3rd intensity pattern, denoted by a central maximum and a single dark ring, appears at 1.1 V in the presence of the edge-bound isophorone, but moves to 1.2 V after molecular desorption. Similarly, the 5th QWS,

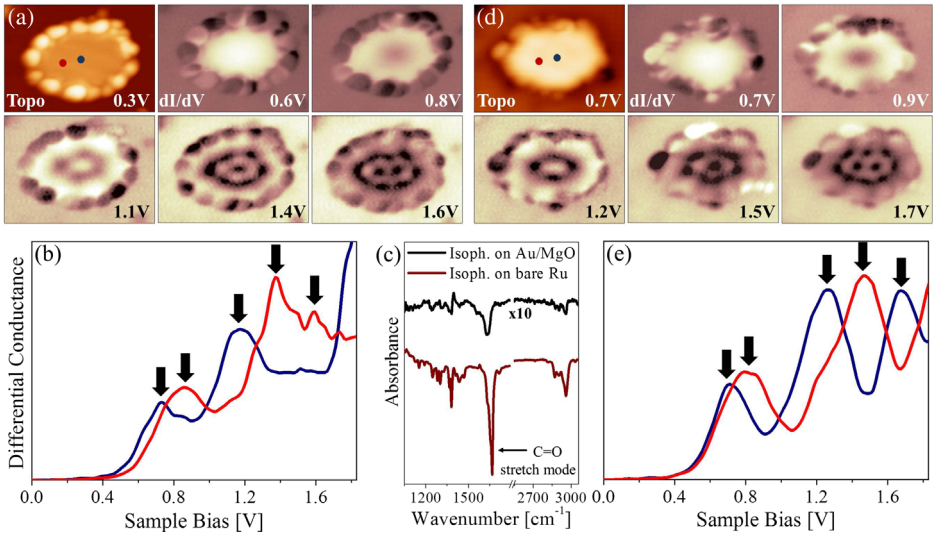

FIG. 2 (color online). Topographic and dI/dV maps of an Au island (a) with and (d) without isophorone molecules bound to its perimeter (11×8 nm^2, 70 pA). (b) and (e) associated conductance spectra taken in the center (blue) and the left part of the island (red) as indicated in (a) and (d). Gaussian fitting revealed five QWSs that are marked by arrows. Their bias positions match the ones used for dI/dV imaging in (a) and (d). (c) Infrared absorption spectra of isophorone adsorbed on Au/MgO (black) and Ru(0001) (gray). Similar vibrational modes are resolved in both cases, indicating that the molecule adsorbs associatively on the two surfaces.

displaying two central minima, experiences an upshift from 1.6 to 1.7 eV after removing the adsorbates. The effect becomes clearer in Gaussian deconvolutions of the dI/dV spectra taken before and after isophorone desorption [Figs. 2(b) and 2(e)]. While the first QWS appears at slightly lower bias, the following ones shift upwards. The energy difference follows an almost linear relationship as a function of the quantum number n, and the $E(n)$ dispersion features a 25% larger slope for the pristine than the isophorone-covered deposit (Fig. 4). Although details of the energy shift vary from cluster to cluster, the slower rise of the QWS dispersion upon molecular adsorption has been reproduced in several cases.

Interestingly, CO_2 dosage onto the Au islands yields the opposite effect. Despite lower data quality, characteristic eigenstates of the deposits could be identified with and without CO_2 species again (Fig. 3). In contrast to isophorone, the pristine island shows a systematic downshift of the QWSs with respect to the CO_2-covered system. The energy change is small for the lowest QWS, but increases linearly with quantum number n to about 0.5 eV for the 4th state. In terms of the dispersion relation, this translates to a 30% steeper slope in presence of CO_2, just opposite to the trend revealed for isophorone [Figs. 4(a) and 4(b)].

To analyze the origin of the adsorbate-induced electronic perturbation, we have described the Au QWSs with a particle-in-a-box-model [20,27]. In first approximation, the particle shape resembles a distorted hexagon, reflecting the threefold symmetry of the underlying Au(111) lattice [11]. For a hexagonal potential with infinite walls, the energy E of the eigenstates depends linearly on the quantum number n renormalized by the effective electron mass m_{eff} and the quantization area Ω: $E_n = E_0 + (n/m_{\mathrm{eff}}\Omega^*)$ [28]. Note that for potential shapes that are separable into independent x and y components, a parabolic $E(n)$ dispersion relation is obtained as found for chain-like and rectangular metal aggregates [12,20]. The linear dispersion expected for a hexagonal well is fairly reproduced in our experimental data, which indeed shows a regular spacing of eigenstates in both, pristine and adsorbate covered islands (Fig. 4). Apparently, the molecular binding affects mainly the slope of the dispersion, indicating that the effective electron mass and/or the size of the confining potential gets perturbed upon adsorption.

Gold islands saturated with edge-bound CO_2 exhibit a 30% larger slope of the $E(n)$ dispersion than their pristine counterparts. This implies that either the confining potential, the effective electron mass or both values have decreased during formation of the CO_2-Au bond. CO_2 adsorption to low-work-function surfaces, such as alkali or alkali-modified metals is governed by a charge transfer

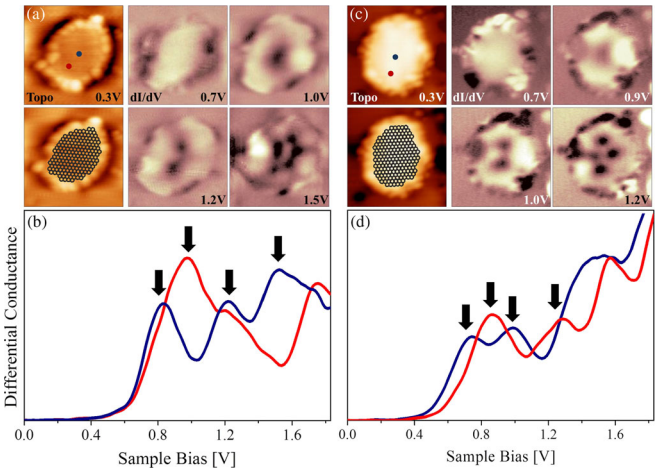

FIG. 3 (color online). Topographic and dI/dV images of an Au island (a) with and (c) without CO_2 molecules bound to its perimeter (8×8 nm^2, 70 pA). Associated dI/dV spectra taken in the island center (blue) and slightly below (red) are shown in (b) and (d). The arrows depict the positions of four QWSs revealed from Gaussian fitting. The respective bias values match the ones used for dI/dV imaging in (a) and (c).

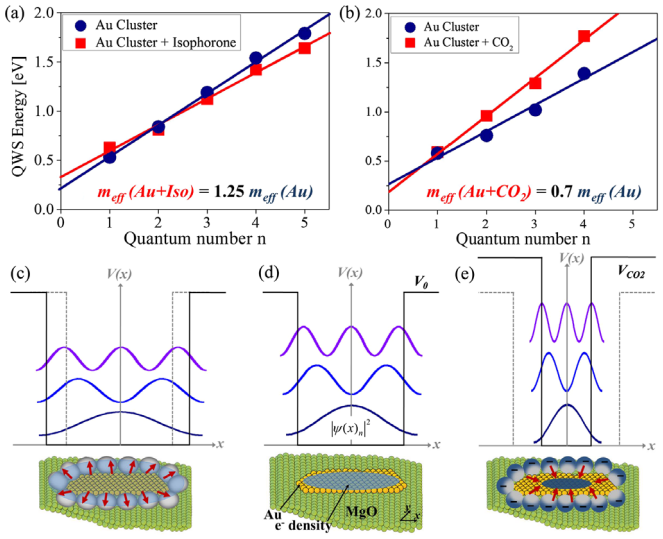

FIG. 4 (color online). Dispersion relation of QWSs in Au islands with/without (a) isophorone and (b) CO_2. The modified $E(n)$ slope can be translated into different effective electron masses that become larger in presence of isophorone but smaller after CO_2 adsorption. 1D scheme showing the electron confinement in (c) an Au island with isophorone, (d) a pristine island and (e) an island with edge-bound CO_2. Attractive isophorone-Au forces promote electron spill-out in (c), which increases the potential well and causes the QWSs to move together. Conversely, charge transfer into the CO_2 generates a repulsive rim around the island that results in a compression of the Au electron gas and moves the QWSs apart (e).

towards the adsorbate, resulting in the formation of CO_2^- or oxalate species; i.e., two CO_2^- hold together by a C-C bond [29]. On neutral Au islands, such binding scenario is unlikely, given the high electronegativity of gold and the appreciable activation barrier for electron transfer into the CO_2 (0.6 eV) [30]. This situation changes, however, on the negatively charged islands on MgO thin films that have accumulated roughly 0.2 extra electrons per interfacial Au atom according to DFT calculations [11]. The extra electrons reside almost exclusively along the island perimeter, where a high density of Au anions was identified by spectroscopic means [31]. Such electron-rich aggregates are suitable for electron transfer into the CO_2 species. The electron exchange enhances the CO_2 binding strength and reduces the electrostatic repulsion between Au^- edge ions, both effects lowering the energy barrier for charge transfer into the CO_2. In fact, oxalate species have been detected by infrared absorption spectroscopy (IRAS) on the Au/MgO system after CO_2 dosage, confirming the accessibility of the above binding scheme [14]. We note that a similar adsorption mechanism has been identified also for O_2 on the monolayer Au islands, driven by the high Lewis acidity of molecular oxygen in that case [32].

Based on the electron transfer from perimeter Au atoms into the CO_2 molecules, we propose the following scenario for the observed reorganization of the gold QWSs [Fig. 4(e)]. The Au atoms in direct contact with CO_2 lose one valence electron towards the ligand, which affects their ability to hybridize with the $6sp$ orbitals of the inner atoms and to contribute to the QWSs [33,34]. The negatively charged CO_2, on the other hand, exerts repulsive forces on the remaining electron cloud that further contracts due to a positive net charge in the island center after electron transfer. The sum of these contributions causes the electron cloud in the gold to contract and the quantization area Ω to decrease [Fig. 4(e)]. Moreover, a higher electron density in the remaining volume facilitates exchange and hopping of the delocalized carriers, which in turn lowers their effective mass. Hence, the two key parameters that govern the $E(n)$ dependency are expected to decrease during CO_2 adsorption, explaining the steeper dispersion relation with respect to pristine islands.

Isophorone has a different impact on the islands electron gas, as the slope of the dispersion decreases in presence of the organic molecules. Isophorone is not expected to interact strongly with gold. Its terminal oxygen, as the negative charge center of the molecule, avoids the electron-rich island perimeter in order to minimize Coulomb repulsion. Conversely, the positive molecular center that would benefit from Coulomb attraction to the Au^- is localized at the C=C double bond in the molecular ring and cannot approach the gold due to steric repulsion imposed by the side groups. Substantial Au-isophorone coupling is only expected if the molecular oxygen would be stripped off and replaced by a Au atom, for instance in a dissociative interaction with an O vacancy in the MgO. However, we have no experimental evidence for such a dissociative binding of isophorone. In fact, IRAS data were found to be identical on Au/MgO and pristine Ru(0001) that is known to bind the molecule in an associative manner [Fig. 2(c)] [14]. Moreover, the required O defects develop preferentially at step edges of the oxide film, hence spatially separated from the Au islands that nucleate inside the oxide terraces [35].

In the absence of direct chemical or electrostatic coupling, the Au-isophorone interaction will be governed by van der Waals forces and hydrogen bonding ($Au^{\delta-}$–$H^{\delta+}$). The weakness of these binding schemes is in agreement with the easy removal of the organic molecules from the Au islands with the STM tip, as compared to CO_2. Also, the observed alteration of the Au QWS structure points to a weak, mostly dispersive interaction of isophorone. In fact, a reduced slope of the $E(n)$ dispersion indicates either a larger quantization area or a higher effective mass after adsorption. Both scenarios are compatible with the depolarizing influence of the organic entities onto the Au^- ions at the island perimeter [19]. As a result, repulsive forces imposed by the edge ions diminish and the electron gas is able to spread beyond former boundaries. In addition, the organic molecules might reduce the height of potential walls around the metal island, promoting again the effect of electron spill out [Fig. 4(c)]. Physisorptive interaction of isophorone therefore leads to an expansion of the confining potential, followed by a dilution of the Au electron gas and an increase of its

effective mass. An observable consequence of this perturbation is a smaller energy separation of the Au QWSs, in agreement with the experimental results. The above concepts are well established in plasmon theory under the synonym "interface damping," where they describe the redshift of particle plasmons in the presence of a ligand shell [36].

In conclusion, the quantized electronic structure of ultrasmall Au islands has proven to be a sensitive indicator for adsorption and charge-transfer processes at their surface. Strong binding of molecular ligands associated with a charge transfer out of the islands results in a reduced confinement region, which causes the eigenstates to move apart and the QWS dispersion to become steeper. Conversely, a mostly dispersive interaction promotes the spill out of the islands electron gas, resulting in a flatter $E(n)$ dispersion relation. These two scenarios have been exemplarily discussed for chemisorbed CO_2 and physisorbed isophorone attached to the perimeter of MgO-supported Au deposits.

The perturbation of a confined electronic system by molecular adsorbates is not only of academic interest, but directly affects our understanding of heterogeneous catalysis. In many cases, ground-state properties are used to analyze the role of catalyst particles in chemical processes, although their quantum structure gets modified under reaction conditions. Our experiments demonstrate how the impact of molecular ligands on the properties of metal nanostructures can be investigated on a mechanistic level.

The authors thank the DFG for financial support within the Excellence Cluster "UNICAT." C. S. is grateful for a fellowship of the "Sudienstiftung des Deutschen Volkes." F. C. thanks the Humboldt Foundation for a Georg-Foster Fellowship.

*Corresponding author.
niklas.nilius@uni-oldenburg.de

[1] G. Ertl, H. Knözinger, and J. Weitkamp, *Handbook of Heterogeneous Catalysis* (Wiley-VCH, New York, 2008).
[2] U. Landman, B. Yoon, Ch. Zhang, U. Heiz, and M. Arenz, Top. Catal. **44**, 145 (2007).
[3] M. Haruta, S. Tsubota, T. Kobayashi, H. Kageyama, M. J. Genet, and B. Delmon, J. Catal. **144**, 175 (1993).
[4] M. Valden, X. Lai, and D. W. Goodman, Science **281**, 1647 (1998).
[5] M. S. Chen and D. W. Goodman, Science **306**, 252 (2004).
[6] H.-J. Freund, Catal. Today **238**, 2 (2014).
[7] H. Chen, L. Wu, L. Zhang, Y. Zhang, and C. P. Grey, J. Am. Chem. Soc. **133**, 262 (2011).
[8] P. Y. Huang, S. Kurasch, A. Srivastava, V. Skakalova, J. Kotakoski, A. V. Krasheninnikov, R. Hovden, Q. Mao, J. C. Meyer, J. Smet, D. A. Muller, and U. Kaiser, Nano Lett. **12**, 1081 (2012).
[9] M. F. Crommie, C. P. Lutz, and D. M. Eigler, Science **262**, 218 (1993).
[10] J. Li, W.-D. Schneider, R. Berndt, and S. Crampin, Phys. Rev. Lett. **80**, 3332 (1998).
[11] X. Lin, N. Nilius, H.-J. Freund, M. Walter, P. Frondelius, K. Honkala, and H. Häkkinen, Phys. Rev. Lett. **102**, 206801 (2009).
[12] C. Stiehler, Y. Pan, W.-D. Schneider, P. Koskinen, H. Häkkinen, N. Nilius, and H.-J. Freund, Phys. Rev. B **88**, 115415 (2013).
[13] N. Lopez and J. K. Norskov, J. Am. Chem. Soc. **124**, 11262 (2002).
[14] F. Calaza *et al.*, Angew. Chem., Int. Ed. Engl., doi:10.1002/anie.201501420 (2015).
[15] M. Salmeron and R. Schlögl, Surf. Sci. Rep. **63**, 169 (2008).
[16] J. Wollschläger, J. Viernow, C. Tegenkamp, D. Erdös, K. M. Schröder, and H. Pfnür, Appl. Surf. Sci. **142**, 129 (1999).
[17] S. Schintke, S. Messerli, M. Pivetta, F. Patthey, L. Libioulle, M. Stengel, A. DeVita, and W. D. Schneider, Phys. Rev. Lett. **87**, 276801 (2001).
[18] G. Pacchioni, L. Giordano, and M. Baistrocchi, Phys. Rev. Lett. **94**, 226104 (2005).
[19] X. Lin, N. Nilius, M. Sterrer, P. Koskinen, H. Häkkinen, and H.-J. Freund, Phys. Rev. B **81**, 153406 (2010).
[20] N. Nilius, T. M. Wallis, and W. Ho, Science **297**, 1853 (2002).
[21] See Supplemental Material at http://link.aps.org/supplemental/10.1103/PhysRevLett.115.036804 for the methodology to determine QWS energies and further examples, which includes Refs. [22–24].
[22] I.-P. Hong *et al.*, Phys. Rev. B **80**, 0814091(R) (2009).
[23] J. Repp, G. Meyer, S. Paavilainen, F. E. Olsson, and M. Persson, Phys. Rev. Lett. **95**, 225503 (2005).
[24] N. Nilius, T. M. Wallis, and W. Ho, J. Phys. Chem. B **109**, 20657 (2005).
[25] J. I. Pascual, N. Lorente, Z. Song, H. Conrad, and H.-P. Rust, Nature (London) **423**, 525 (2003).
[26] The eccentricity, as a pivotal parameter for the position of QWSs in monolayer Au islands according to Ref. [12], agrees within 0.1 for pairs of pristine and CO_2-covered deposits as selected in our analysis.
[27] J. Li, W.-D. Schneider, S. Crampin, and R. Berndt, Surf. Sci. **422**, 95 (1999).
[28] In the original Ref. [27], the dispersion is expressed as $E_n = E_0 + (\lambda_n/m_{\text{eff}}\Omega)$. In first approximation, the eigenvalues λ_n can, however, be fitted with $\lambda_n = 10.8n + 5.9$, yielding the equation given here.
[29] F. M. Hoffmann, M. D. Weisel, and J. Paul, Surf. Sci. **316**, 277 (1994); T. Seyller, D. Borgmann, and G. Wedler, Surf. Sci. **400**, 63 (1998).
[30] K. O. Hartman and I. C. Hisatsune, J. Chem. Phys. **44**, 1913 (1966); R. N. Compton, P. W. Reinhardt, and C. D. Cooper, J. Chem. Phys. **63**, 3821 (1975); J. Pacansky, U. Wahlgren, and P. S. Bagus, J. Chem. Phys. **62**, 2740 (1975).
[31] X. Lin *et al.*, J. Am. Chem. Soc. **132**, 7745 (2010).
[32] P. Frondelius, H. Häkkinen, and K. Honkala, Angew. Chem., Int. Ed. **49**, 7913 (2010).
[33] N. Nilius, T. M. Wallis, and W. Ho, Phys. Rev. Lett. **90**, 186102 (2003).
[34] H. Häkkinen, M. Walter, and H. Grönbeck, J. Phys. Chem. **110**, 9927 (2006).
[35] M. Sterrer, M. Nowicki, M. Heyde, N. Nilius, T. Risse, H.-P. Rust, G. Pacchioni, and H.-J. Freund, J. Phys. Chem. B **110**, 46 (2006).
[36] H. Hövel, S. Fritz, A. Hilger, U. Kreibig, and M. Vollmer, Phys. Rev. B **48**, 18178 (1993).